

## RESEARCH ARTICLE

# Height Estimation at Entrance With Passive RFIDs: Possibility, Design and Implementation

YUQIU ZHAO<sup>1</sup>, JIANCHAO LI<sup>2</sup>, AND WENYUAN LIU<sup>1</sup> 

<sup>1</sup>College of Computer and Information Engineering, Central South University of Forestry and Technology, Changsha 410004, China

<sup>2</sup>Key Laboratory of Software Engineering of Hebei Province, School of Information Science and Engineering, Yanshan University, Qinhuangdao 066004, China

Corresponding author: Wenyuan Liu (wylu@ysu.edu.cn)

This work was supported in part by the National Natural Science Foundation of China (NSFC) under Grant 61672448, Grant 61702440, and Grant 61772453.

**ABSTRACT** The height of an entrant is a critical parameter for many practical applications, e.g., the electrical controlling in smart homes and personalized recommendation in smart clothing stores. This paper explores the possibility, design and implementation of estimating the entrant's height with low-cost passive RFID tags deployed in the entrance zone (e.g. the doorway). Taking the signal RSSI measurements as the input, we first identify the signal frames influenced by entrant's passing through, and then convert the identified frames into a strength image, so that the his/her height can be estimated using a simple yet effective image analysis algorithm. We implement a prototype system of RFH with COTS RFID devices, and conduct extensive experiments to validate our design. The experimental results demonstrate that our scheme is able to achieve more than 80% acceptable accuracy in various scenarios with different parameter settings.


**INDEX TERMS** Height estimation, RFID, entrance sensing, strength image.

## I. INTRODUCTION

The past decades have witnessed the prevalence of Radio Frequency Identification (RFID) in numerous practical applications. With the merits of wireless communication, high reading rate, low cost and easy deployment, passive RFID tags (RFIDs) are attached on commodities in retail stores, packages in logistics systems and books in libraries, so that their information can be identified and recorded at the back-end server, and can significantly improve the management accuracy and efficiency.

Beyond the traditional identification, there is a clear trend of turning RFIDs into one of wireless sensing technologies in recent years. The two hottest topics are RFID localization and tracking [1]–[4], activity and behavior recognition [5]–[9], which have attracted much attention from both academic and industrial communities. Besides, there are also many excellent works on mechanical vibration period sensing [10], spinning sensing [11], heart and breath rate sensing [12], and etc.

In our daily life, the entrant's height is a critical and important parameter. Many applications will be benefited from an

The associate editor coordinating the review of this manuscript and approving it for publication was Marco Martalo .

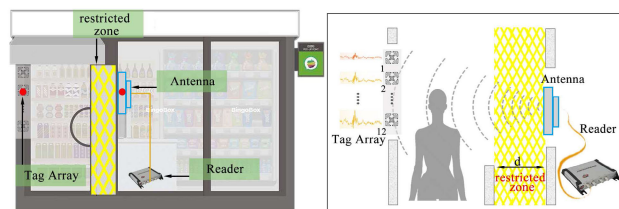


**FIGURE 1.** System composition and possible application in unmanned store.

accurate height estimation. For example, when a customer enters the clothing store, the salesman can give out precise clothing size recommendation if his/her height can be accurately estimated. According to the estimated height, we can intelligently adjust the light luminance over the sofa in a smart home system. Both video [13] and smartphone [14] based methods have great limitations. The video based approaches are sensitive to the light conditions, and suffer from the issues of blocking and privacy leakage risk. While the smartphone based approaches require the user to keep stably for a period of time during the height detection, which may cause congestion at the doorway and hence impractical.

With the promising RFIDs, in this paper, we take the entrant's height estimation, which is primary important for many applications as the goal. To our best of knowledge, it is a completely new and open problem which cannot be well resolved by existing object shape [15] and material [16] detection methods. We propose a device-free and non-intrusive height estimation solution called as RFH, to identify and approximate the entrant's height with low-cost passive RFID tags. The main setting up of RFH is shown in Fig.1, which consists of an antenna connected to an ImpinJ reader and an array of  $k$  ( $k = 12$  in our experiments) vertically deployed tags. The intuition behind RFH is that the presence of entrant between antenna and array will cause different impacts to the backscattered signals of the tags in the array. So it is possible for us to estimate the entrant's height according to the signal measurement differences of tags.

However, it is not so easy to achieve this and there are several challenges which should be coped with well. First, how to distinguish the boundary which can reflect the entrant's height accurately, since the presence of entrant will influence the signal propagations of all the tags in the array. Second, how to eliminate the impact of device diversity so as to guarantee the easily deployment and transfer capability of our RFH in different scenes.

The contributions of our work can be summarized as follows:

- To our best of knowledge, we are the first to estimate entrant's height with low-cost RFID tags. And a device-free solution called as RFH is proposed according to the entrant's influence differences between tags.
- We propose a novel fusion approach to identify the influenced signal frames for entrant's presence, and an image transformation method is adopted to transform these frames into a strength image, so that the entrant's height can be estimated accurately with a lightweight yet effective image analysis.
- We design and implement a prototype of RFH using COTS RFID devices without any hardware modification. We also evaluated its performance via extensive experiments. The results demonstrate that our RFH can estimate entrant's height with an accuracy of more than 80%.

This paper is organized as follows. We first discuss and summary the related works in Section II. Then, Section III extensively introduces background and problem formulation. Next, we give out the detail design of RFH in Section IV. The implementation of RFH and experimental evaluation results are described in Section V. Finally, this paper is concluded by Section VI.

## II. RELATED WORK

Non-intrusive human associated sensing has been one of the hottest topics in recent years. A school of approaches and methods have been proposed. Existing works can be catego-

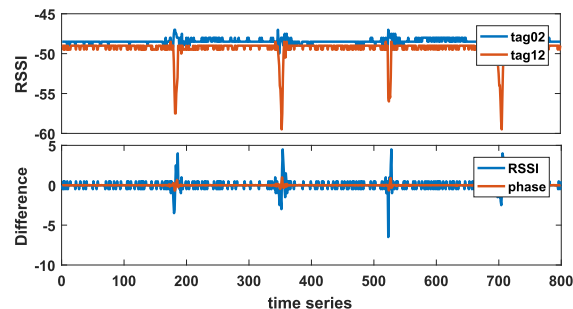


FIGURE 2. Experimental observations.

rized into three categories, i.e., image based methods, WiFi based methods and RFID based methods.

### A. VIDEO AND IMAGE BASED METHODS

Most of recent image based methods mainly focus on pose detection [17] and gesture recognition [18], and the height estimation problem is out of their scope. To estimate the human pose and shape from images, model-based works [19] use a parametric body model or template. Recent methods typically predict 3D keypoints or stick figures from a single image using the CNN. Pavlakos *et al.* [20] take another approach by relying on weak 3D supervision in form of a relative 3D ordering of joints. Some works [21] regress correspondences to a body model which are used to fit the model to depth data. Chu *et al.* [22] presents self portrait interface using vision-based hand motion gesture. Their research makes it possible for users to manipulate digital camera when taking self-portrait pictures. Madhuri *et al.* [23] presents a vision based sign language translation device. Raheja *et al.* [24] proposed a method to recognize and track fingertips and center of palm using Kinect.

### B. WiFi BASED METHODS

Recently, CSI measurements from WiFi systems are used for different sensing purposes [25]. WiFi sensing reuses the infrastructure that is used for wireless communication, so it is convenient to deploy and low cost. The CSI amplitude variations will present different patterns to different users, activities, gestures, and so on, which makes it can be used to achieve human presence detection [26], fall detection [27], motion detection [28], activity recognition [29], gesture recognition [30]. Moreover, the CSI phase can be used for accurate human localization and tracking [31] and breathing rate estimation [32]. FormaTrack in [33] employs the signal doppler of mmWave to identify body shape.

### C. RFID BASED METHODS

There is also a trend of turning RFID into wireless sensing system in recent years. Tadar [34] tracks moving objects by establishing a multi-antenna system with RFID tags and analyzes the signals reflected from moving objects.  $i^2tag$  [9] analyzes multi-information with multidimensional dynamic time warping-based algorithm to achieve recognition of four types

of exercises. TagBreath [35] and [36] achieves detection of breathing and body temperature using RFIDs. Tagsheet [37] tries to capture and identify the body postures during sleeping with the image information derived from reflected signals.

### III. PRELIMINARIES

#### A. RSSI MEASUREMENT OF RFID

Without their own power supplies, passive tags only can backscatter and modulate their data into the reader's signal [38]. COTS RFID reader, such as ImpinJ 420, are able to report signal measurements like RSSI, phase and doppler-shift for the purpose of batteryless sensing. Referring to [7], the received RSSI of a specified tag can be modeled as

$$RSSI = 10\log_{10}P, \quad (1)$$

where  $P$  is the sum of the power (in mW) received by the reader.

In an indoor environment, the transmitted signal and the backscattered signal propagate to the receiver through multiple paths. Each path contributes with a differently delayed, attenuated, and phase-shifted signal. Hence, the received signal is a combination of numerous alias versions of the original signal. Therefore, the received power  $P$  can be denoted as

$$P = \sum_{i=1}^N P_i, \quad (2)$$

where  $P_i$  is the power of  $i$ th multipath component and  $N$  is the total number of components. Obviously,  $P_i$  is hypersensitive to the propagation distance of  $i$ th multipath signal.

However, it is challenging and almost impossible to decompose the received signals into different multipath signals. For simplicity, we can decompose it into two components as many existing works do as

$$P = P_{los} + P_{nlos}, \quad (3)$$

where  $P_{los}$  and  $P_{nlos}$  are the line-of-sight (LOS) and non-line-of-sight (NLOS) components respectively. And the  $P_{los}$  is the main component as declared in literatures. The blocking of LOS caused significant decline to the received power, and hence large RSSI variation. While the blocking of NLOS only causes small RSSI decline. Fig.2 presents the RSSI variation patterns when an entrant passes through the intermediate region between reader and tags. Fig.2 also shows the one selected tag's RSSI and phase differences between dynamic and static scenes. We can observe from the figure that the RSSI declining is indeed hypersensitive to the entrant's position as we expected. This characteristic inspires and motivates us to estimate the entrant's height by leveraging the changes of tags' RSSI.

#### B. PROBLEM FORMULATION

Considering in a smart physical space, e.g., a smart retail store or a smart home, RFID devices are deployed for the purpose of ambient sensing. Particularly, a reader antenna and an array of tags are deployed at the two sides of the entrance

as shown in Fig.1. The reader repeatedly interrogates tags and reports their RSSIs for each identification reading. The tags are laid out in a vertical column with 5cm spacing between two adjunct ones.

When someone passing through the doorway, the presence of entrant influences the signal propagations of all tags, and hence leads to the RSSI changing and variation. However, the presence of entrant only will block the LOS paths of some tags (the tags behind entrant's body), and block the NLOS paths of others (the tags over entrant's head). Such phenomenon will cause different RSSI changing pattern to the tags in the array. So there is a chance for us to estimate his/her height approximately according to the differences between tags.

Moreover, we assume that the entrant's height is in the range of 1.25m to 2m, the tag array is deployed with a height of 1.25m from the ground. We also assume that the walking speed of entrant is not so fast, and it is in the range of 0.9-1.2m/s. With 12 tags in the array, we can collect 8.33 data samples per second under the sampling rate of 100 times per second. We believe that such sample rate is already enough to achieve relatively high accuracy. So that these two assumptions are reasonable for practical application, which will guarantee the availability of our proposal in practice.

### IV. SYSTEM DESIGN

In this section, we give out the detailed design of RFH to estimate entrant's height via RSSI strength imaging.

#### A. SYSTEM OVERVIEW

As aforementioned, our goal is to estimate the entrant's height when someone passing through the sensing zone of deployed RFID devices. Fig.3 presents the overall architecture of RFH. As shown in the figure, our RFH consists of four steps with signal RSSI as inputting and with height estimation result as outputting.

The first step is data collection. The reader repeatedly interrogates tags using only one antenna and produces a stream of readings in its sensing zone. Then, the preprocessing step eliminates the location-aware strength with an average subtraction, interpolates the misreadings and aligns the RSSIs of tags by time. In the third step, called influenced frame identification, variance-based features are extracted and fused to identify the influenced frame of the entrant passing through. To estimate the entrant's height, the RSSIs of identified frames are converted to a strength image in the last image analysis step.

#### B. PREPROCESSING

##### 1) MISREADING INTERPOLATION

RFID is a typical central network, which means that the tags can not communicate with each other. Tags can only use TDMA mechanism to avoid collision. So there are always identification collisions at reader side. The TDMA mechanism will lead to there are always random misreading during

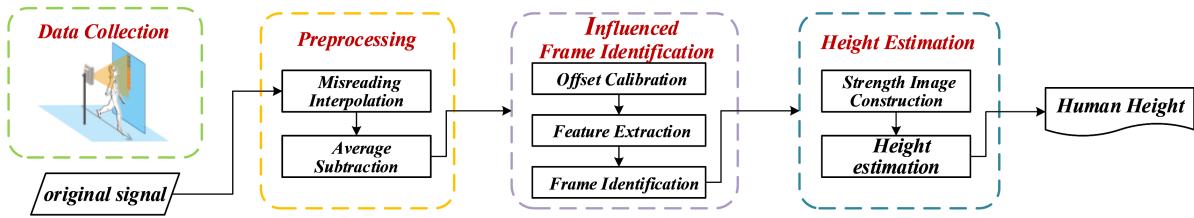


FIGURE 3. System overview.

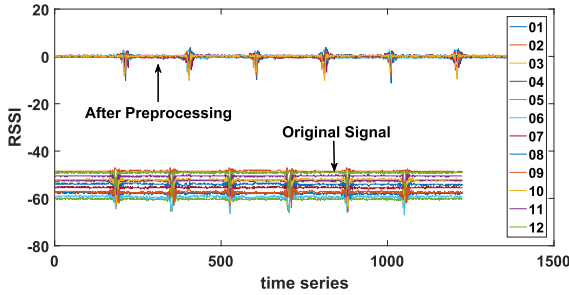


FIGURE 4. The signal before/after preprocessing.

the interrogation. To address this issue, we interpolate such misreading RSSI with previous one of last reading sample.

2) AVERAGE SUBTRACTION

One more thing, as the reader antenna and tag array are deployed on the two sides of door, the distances between each tag and antenna are different from each other. In other words, the received RSSIs is location-aware. Since we only concern tags' change patten rather than the absolute RSSI values, the distance differences should be eliminated. To achieve this goal, we first randomly select 200 samples from the static setting (without passing through) of every tag's reading stream, and calculate their means. For each tag, we let the original RSSIs subtract its own mean to eliminate the influence of location difference. After the subtraction, the RSSI measurements is close to 0 when there is no entrant's presence, while the change patten when there is entrant's presence are preserved for further analysis. Fig.4 plots the RSSI stream of all 12 tags before and after preprocessing.

C. INFLUENCED FRAME SEGMENTATION

After preprocessing, we try to identify the influenced frame which embraces the whole passing through behavior. The key of frame segmentation is to accurately get the start and end time of passing through.

1) OFFSET CALIBRATION

As shown in Fig.5, the preprocessed signals may still contain small offset caused by various noises, such as the thermal and environment noises.

If we define the preprocessed signals of arbitrary *i*th tag as  $\{x_1^i, x_2^i, \dots, x_t^i, \dots\}$ , where  $x_t^i$  denotes the preprocessed RSSI

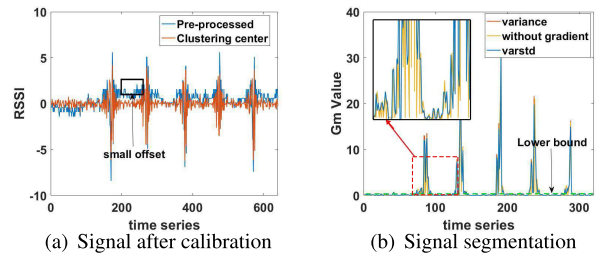


FIGURE 5. Influenced frame segmentation.

value of tag *i* at time *t*, we can calibrate the  $x_t^i$  with a sliding window whose width is *w* as

$$cx_t^i = x_t^i - \frac{1}{w} \sum_{j=t}^{t+w} x_j^i, \tag{4}$$

where  $cx_t^i$  is the calibrated results of  $x_t^i$  and the value of *w* can be tuned according to the average walking speed of entrants to adapt different scenarios. In our experiments, we empirically set it to be 4.

After that, the well known Savitzky-Golay smoothing [39] is performed to further remove the random noises. And the Fig.5(a) presents the results after the calibration.

2) FEATURE EXTRACTION

With the calibrated RSSI stream, we then calculated the time series variances and standard deviations using another sliding window as,

$$\begin{cases} Var_{nt}^i = \frac{1}{wl} \sum_{t=nt}^{nt+wl} (cx_t^i - \overline{cx}^i)^2 \\ Std_{nt}^i = \sqrt{Var_{nt}^i} \end{cases} \tag{5}$$

where *nt* is the time index and *wl* is the window length whose value is set to be 2 in our experiment.

In order to eliminate excessive glitches in the signal, we use traditional gradients to smooth the data. The purpose of using gradients is also to eliminate the impact of data between the time points before and after. In addition, we define both variance gradient and standard deviation gradient between two adjacent sliding windows as new variables:

$$\begin{cases} \Delta Var_{nt}^i = |Var_{nt+1}^i - Var_{nt}^i| \\ \Delta Std_{nt}^i = |Std_{nt+1}^i - Std_{nt}^i| \end{cases} \tag{6}$$

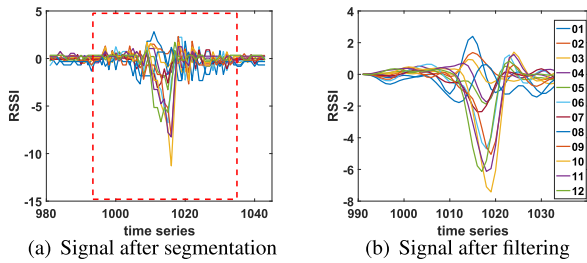


FIGURE 6. Signal extraction.

Considering the influence of variance and deviation synthetically, we set the weighting coefficient  $a$  and define the formula as follow,

$$G_{nt}^i = a\Delta Var_{nt}^i + (1 - a)\Delta Std_{nt}^i. \quad (7)$$

It should be noted that both the weighting coefficient and window length are supposed to be precisely adjusted according to the walking speed. In our experiment, we empirically set  $a$  to be 0.9 for more accurate segmentation.

The extracted feature  $G_{nt}^i$  from one tag may embrace false positive. To enhance the frame identification accuracy, we fuse features from all the tags together as

$$G = \sum_{i=1}^n G_{nt}^i, \quad (8)$$

where  $n$  is the total number of tags in the array. With such fusion, the influence of entrant's presence is amplified, which is helpful for frame identification. Fig.5(b) plots the fused  $G$  with six passing through. As shown in the figure, the stationary portion and the influenced portion can be clearly distinguished for further frame identification.

### 3) FRAME IDENTIFICATION

With the extracted feature  $G$ , we then identify the frame boundary (i.e., start and end points) of passing through using a heuristic threshold based method. In detail, we first calculate the histogram which describes the distribution of  $G$ .

Since the values without entrant's presence are always smaller than those with entrant's presence, the first component of histogram can be ignored and the minimum value of the second component can be regard as the wanted threshold.

We define this threshold as the lower bound. If the values in  $G$  are smaller than this lower bound, we can determine that they must be static states without entrant's presence. Otherwise, when the values are larger than the lower bound, they must be dynamic states with entrant's presence. Hence we can take the first point whose value is larger than the lower bound as the start point of the frame and the following last point whose value is larger than the lower bound as the end point of the frame. In such way, we can get the wanted frame accurately as the red rectangle shown in Fig.5(b).

With this identified frame boundary, we can segment the original RSSI streams of all the tags tidily. Fig.6(a) plots the segment results of all the 12 tags. However, it is still

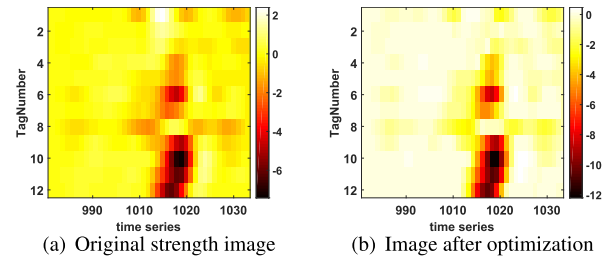


FIGURE 7. Strength image construction.

a challenge for us to estimate the entrant's height according to the segment results. Therefore, we adopt another image-based method to quantitatively characterize the influence of entrant's presence, so that the entrant's height can be estimated accurately as we show in the next subsection. Before that, a Butterworth low-pass filtering is further employed to smooth the segmented original RSSI streams for all the tags, and the results are shown in Fig.6(b).

### D. HEIGHT ESTIMATION

When someone passing through the sensing zone, different presence locations have different influences on all tags in the array, so the influenced frame can be further divided into three parts, weakly influenced part, medianly influenced part and strongly influenced part. Among them, only the third strongly influenced part indicates the blocking of LOS path between reader and tags, and can be used for height estimation. How to identify the third part, namely centrum identification, is another problem which we should cope with well. To achieve this, we convert the influenced frame into a strength image, and estimate the entrant's height with a image processing method.

#### 1) STRENGTH IMAGE CONSTRUCTION

Supposing there are  $n$  tags, and the length of influenced frame is  $m$ , we can project them into a strength image as follows:

$$I = \begin{pmatrix} x_{1,1} & x_{1,2} & \cdots & x_{1,m} \\ x_{2,1} & x_{2,2} & \cdots & x_{2,m} \\ \vdots & \vdots & \vdots & \vdots \\ x_{n,1} & x_{n,2} & \cdots & x_{n,m} \end{pmatrix}, \quad (9)$$

where  $x_{i,j}$  is the strength of  $i$ th tag at the time of  $m$ . In the image, each row is uniquely mapped to a same tag. The mapping fashion between the tags and rows is identical to the vertical order from up to down in the deployed tag array. Fig.7(a) presents a typical example of strength image for one passing through.

Unfortunately, the image is not so perfect as we expected. First, there are always outliers, i.e., the sporadic red pixels as shown in Fig.7(a). Second, the pixels even on the centrum are discontinuous. All these will cause ambiguity to the centrum identification and finally cause error height estimation.

To this end, we introduce an entropy based optimization algorithm (EBOA) in our RFH. We define the entropy for

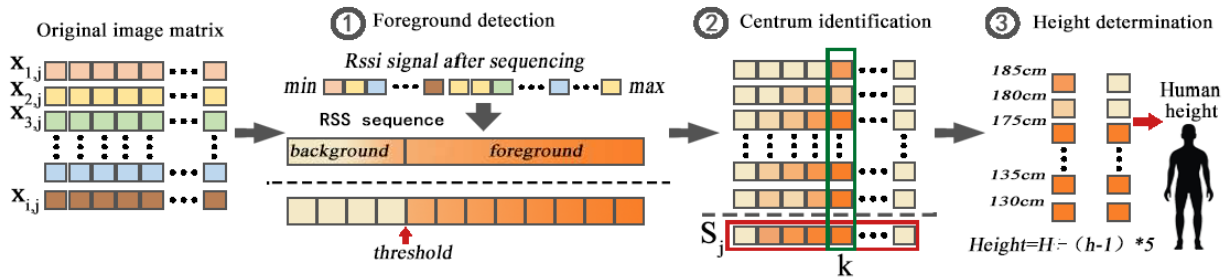


FIGURE 8. Height estimation pipeline.

each pixel as

$$e_{i,j} = x_{i,j} \log_{10} \left( \frac{x_{i,j}}{X_i} \right), \quad (10)$$

where  $X_i = \sum_{j=1}^m x_{i,j}$  is the sum of pixel values of  $i$ th tag.

Then, the pixel synthesis can be calculated as

$$x_{i,j}^{optimal} = x_{i,j} + e_{i,j}, \quad (11)$$

where  $x_{i,j}$  is the original pixel value and  $e_{i,j}$  is the entropy. Fig.7(b) plots the new strength image after optimization. We can see from the figure that most outliers are removed, and the most red pixels are concentrated on the centrum, which is helpful for further centrum identification.

## 2) HEIGHT ESTIMATION

Then, we can estimate the entrant’s height according to constructed strength image. The whole estimation procedure (as shown in Fig. 8) is consisted of three steps: foreground detection, centrum identification and height determination. The goal of foreground detection is to further remove interference, the centrum identification is to find out the most influenced centrum by passing through, and the entrant’s height is estimated in the last height determination step.

**Step 1: Foreground detection:** Foreground detection to segment the foreground pixels from the rest of an image, i.e. background, is a fundamental problem in computer vision, which has been well studied for many years [33]. And the background subtraction is the most popular method for foreground segmentation. While such method is not suitable for our RFH, because we compose the time series RSSI streams of all the tags into a strength image.

To guarantee the system efficiency and achieve real-time height estimation, we adopt a simple yet efficient threshold based method to detect the foreground. We empirically define another threshold here. If any pixel  $x_{i,j}$  in the strength image is larger than the threshold, it is taken as background. Otherwise, it is regard as foreground. For these background pixels, we reset them to be a default value, e.g. 0. And keep the foreground pixels unchanged.

**Step 2: Centrum identification:** To identify the centrum, namely the blocking of LOS, in the image, we calculate the

sum of each column as

$$S_j = \sum_{i=1}^n x_{i,j}, \quad (12)$$

where  $i$  is the index of tag and  $j$  is the index of column in the strength image.

The blocking of LOS caused by passing through will lead to significant influences on all the tags in the array, and hence larger column sum. Therefore, we can take the  $k$ th column which satisfy

$$k = \arg \max_j S_j, \quad (13)$$

as the centrum.

**Step 3: Height determination:** After the centrum identification, we can then approximate the entrant’s height according to the strength distribution on the  $k$ th centrum. The intuition behind it is to find out the highest (minimum) tag index in the foreground pixels of the  $k$ th centrum. That is to say, we want a  $h$  which satisfy

$$h = \arg \min_i x_{i,k}, \quad (14)$$

where  $x_{i,k}$  should subject to  $x_{i,k} < 0$ , which means that  $x_{i,k}$  should be the foreground pixels of the strength image.

Since the deployed height of the tag array is a prior knowledge in our RFH, we can estimate the entrant’s height (in cm) according to the tag index  $h$  as

$$height = H - 5(h - 1), \quad (15)$$

where  $H$  is the height of the tag array whose value is 185cm (1.85m) in our experiments, 5 is the spacing distance (5cm) between two adjacent tags.

## V. PERFORMANCE EVALUATION

### A. IMPLEMENTATION

We implement a prototype of RFH with COTS RFID devices without any hardware modification.

#### 1) HARDWARE

Fig.9 depicts the detailed hardware setup. We employ the Impinj Speedway R420 reader connected with a 8.5dbic gain Alien ALR-8696-L circular polarized antenna to interrogate

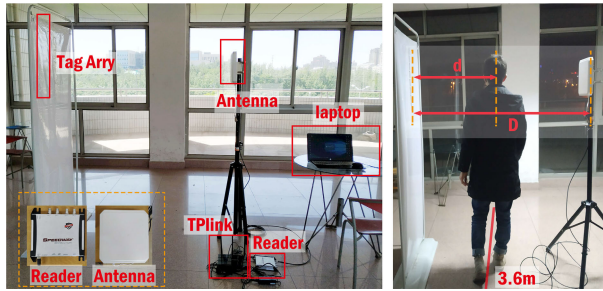


FIGURE 9. Experimental scenes and hardware setup.

TABLE 1. System parameters and default experiment settings.

Parameter	Range	Default
Volunteer	1-12	3rd
Entrant-tag distance	0.3-0.9m	0.3m
Walking speed	0.3-1.2m/s	1.2m/s
Antenna-tag distance	1-2m	1.50m
Antenna height	1.4-1.6m	1.50m
Antenna angle	+45,0,-45	0
Scenario	hall1,hall2,water room	hall1
Tag type	E41-C,AZ-E53,H-47	H-47

passive tags. We also evaluate different types of tags, including Impinj H47, AZ-E53 and E41-C. The tags are deployed in a vertical line, so as to construct a tag array with  $k = 12$  tags. The RFID system operates at the band between 902MHz and 928MHz, and follows the standard EPC protocol. The transmission power of reader is configured to be 30dBm. And the reader reports and sends the low level data to the laptop via Ethernet cable.

## 2) SOFTWARE

We implement RFH based on the public LLRP Toolkit (LTK) with Java in a laptop, which equips a 2.5GHz cpu (i5-7300HQ) and 8GB memory. The reader continuously interrogates tags in the communication range and reports low level data (e.g., RSSI, phase, doppler shift and time stamp) according to the parameter settings of reader. After the data is collected, we analyze and process the data with MATLAB.

## B. EXPERIMENTAL SETUP

As shown in Fig.9, the antenna and tag array are deployed in the fixed locations with a displacement of  $D$ . The value of  $D$  is set to be 1.5m, which is the common width of door in China. To evaluate the performance of RFH, we recruit 12 volunteers, whose heights range from 160cm to 180cm diversely. For each experiment, we ask a volunteer to walk through the entrance zone between antenna and tag array with a distance  $d$  to the tag array in a specific speed, no other requirements are imposed, which means the volunteers can walk in their own styles. Table 1 summarizes key system parameters and default experiment settings.

Since our RFH is the first work towards height estimation in literatures, we mainly compare the performance of RFH with and without EBOA in the strength image construction

step. The estimation accuracy is one of the most important metrics for height estimation, so we employ two typical accuracy metrics to evaluate the performance of our RFH, namely

$$Error = |height_{\text{ested}} - height_{\text{gth}}|, \quad (16)$$

and

$$Accuracy = \frac{n_{\text{right}}}{n_{\text{total}}}, \quad (17)$$

where  $height_{\text{ested}}$  is the estimated height and  $height_{\text{gth}}$  is the height ground truth. Respectively,  $n_{\text{total}}$  is the total number of experiments and  $n_{\text{right}}$  is the number of experiments when the estimation  $Error$  is smaller than 2.5cm. The reason why we calculate the accuracy with Equation 17 is that the spacing distance of two adjacent tags is 5cm, so the estimation output must be times of 5cm in our experiments. If someone wants to improve the estimation accuracy, we can just attach more tags in the tag array so as to reduce the spacing distance of adjacent tags.

## C. IMPACT OF ENTRANT ASSOCIATED PARAMETERS

### 1) IMPACT OF ENTRANT DIVERSITY

We first investigate the impact of entrant diversity to the final height estimation accuracy with different volunteers. All the volunteers are divided into five clusters according to their height as C1 (160-165cm), C2 (165-170cm), C3 (170-175cm), C4 (175-180cm), C5 (180-185cm) respectively. Each volunteer is asked to walk through the entrance zone for 25 times, and their heights are estimated using our RFH for each passing through. Fig.10(a) plots the confusion matrix for all the five clusters. We can see from the matrix that both the C1, C3, C4 and clusters achieve more than 80% estimation accuracy, the accuracy of C4 even reaches up to 100% in our experiments. While the accuracies of C2 are only 48%, which is far away from our expectation. The first reason is that one of volunteer in C2 is too fat to bring significant ambiguity during the centrum identification according to the strength image. The second is that the number of experiments for each volunteer is only 25 times, if more experiments are conducted, the accuracy can be greatly improved.

### 2) IMPACT OF ENTRANT-ARRAY DISTANCE $d$

Then we examine the impact of the walking patten of entrants to the estimation accuracy. Obviously, the distance  $d$  between entrant and tag array is the first influence factor, which we should consider in. With other parameters fixed, we ask the volunteer to pass through the entrance zone with different  $d$  varied from 30cm to 90cm. The estimation accuracy results are shown in Fig.10(b). As shown in the figure, with  $d$  increasing from 30cm to 90cm, our RFH achieve 90% estimation accuracy in average. Particularly, when the distance  $d$  is 30cm, our RFH achieve more than 98% accuracy. Moreover, we can find that The increase in distance is inversely proportional to the accuracy, and the performance with EBOA is better than without EBOA in general. Fig.10(c) presents the

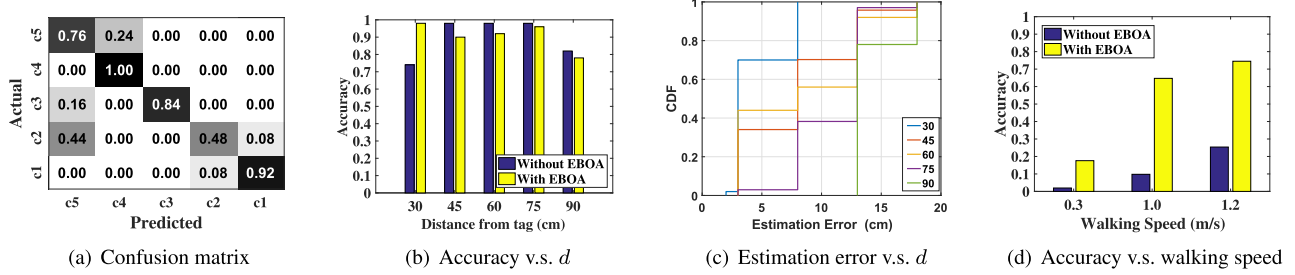


FIGURE 10. Impact of entrant associated parameters.

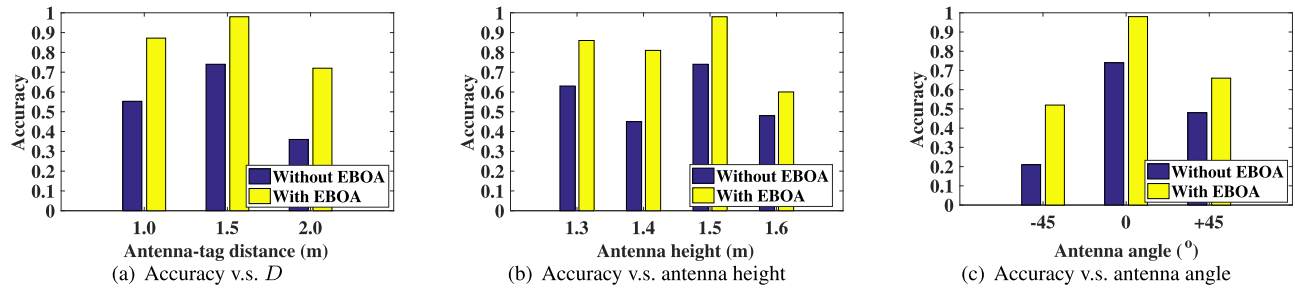


FIGURE 11. Impact of hardware associated parameters.

CDF of estimation error and the performance with EBOA are better than without EBOA in general. when 100 experiments are conducted for each entrant-array distance. We can get from the figure that RFH achieves 2.5cm estimation error in average when the distance is 30cm, and 5cm when  $d$  is 75cm. Such phenomenon can be explained as when the entrant is far away from the tag array and close to the antenna, the body of entrant blocks most of LOS path and emitted signals, which will bring significant ambiguity to the feature extraction and centrum identification of RFH, so finally influence the height estimation accuracy.

### 3) IMPACT OF ENTRANT'S WALKING SPEED

Moreover, the walking speed of the entrant is another key parameter for height estimation accuracy. To evaluate its influence, we asked a volunteer to walk through the entrance zone with specified speeds, 0.3m/s, 1m/s and 1.2m/s respectively. The first 0.3m/s is an extreme slow speed and 1m/s, 1.2m/s are general walking speeds. The volunteer was asked to control his/her walking speed via walking time controlling. The corresponding results are shown in Fig.10(d). As illustrated in the figure, when the walking speed is extremely slow, the estimation results are inaccurate with only 19% accuracy. However, when the walking speed is general, the estimated height is very close to the groundtruth, and RFH achieves more than 82% accuracy. The reason can be that when the entrant walks slowly, the presence of entrant will influence the RSSI signals with a longer time, which brings ambiguity to the centrum identification of final height estimation step. All these suggest that it is better for the entrant to walk closer

to the tag array in a general speed to improve the accuracy of RFH.

## D. IMPACT OF HARDWARE ASSOCIATED PARAMETERS

### 1) IMPACT OF ANTENNA-ARRAY DISTANCE $D$

We then evaluate the performance of our RFH at different distances from antenna to the tag array. In the experiment, we keep other parameters with default values and vary the antenna-array distances  $D$  from 1m to 2m. Fig.11(a) plots the accuracy at different  $D$ . According to the experiment results, the accuracy of RFH height estimation with EBOA is only 85% when  $D=1$ m, and the accuracy is improved to be 72% without EBOA and 98% with EBOA respectively when the distance is 1.5m. When the distance is 2m, the accuracy declines to be 30% without EBOA and 70% with EBOA. The reason can be explained as when the antenna-tag distance is large, the received signal RSSI is so weak that it will cause errors in foreground detection, and finally cause height estimation errors.

### 2) IMPACT OF ANTENNA HEIGHT

Furthermore, we evaluate the height estimation accuracy with different antenna height whose default value is 1.5m. Both the locations of antenna and tag array is fixed, we only change the height of antenna from 1.3m to 1.6m while keep the height of tag array unchanged. Fig.11(b) plots the corresponding experimental results. According to the figure, when the antenna height is 1.5m, our RFH gets the best estimation accuracy around 76% without EBOA and around 97% with EBOA optimization. This is because when the antenna height is



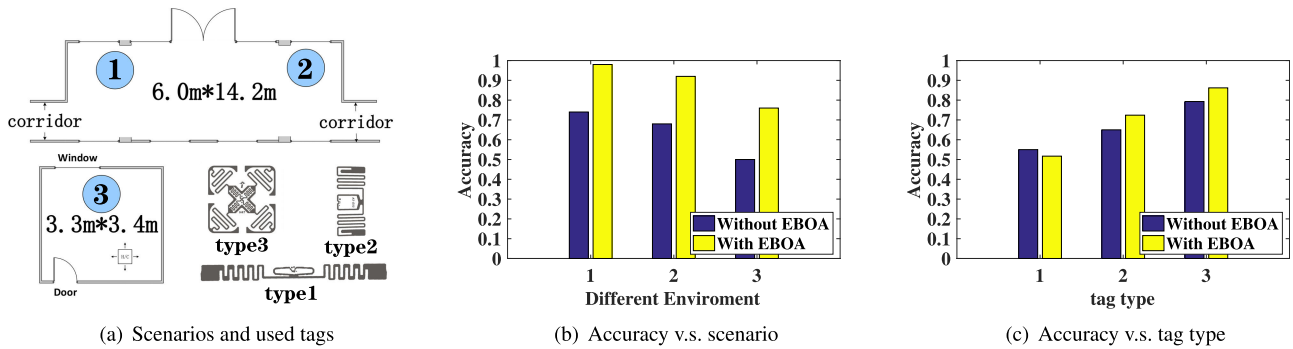


FIGURE 12. Impact of environment associated parameters.

1.5m, the center of antenna is rightly facing the center of the tag array, the passing through of entrant caused equal influence to all tags in the array, so that the accuracy of both foreground detection and centrum identification can be guaranteed.

### 3) IMPACT OF ANTENNA ANGLE

The signals of RFID system are influenced by antenna orientation, which has been widely discussed in many other literatures. The aforementioned performance is achieved with the assumption of the antenna is rightly facing the tag array. Then, we evaluate the height estimation accuracy at different antenna orientation. For this purpose, we keep the tag array fixed and adjusted the angle of antenna to the left and right sides. Fig.11(c) compares the estimation accuracy of three typical antenna angles. We observe that the right facing scheme achieve the best accuracy among all the antenna orientations. Actually, such scheme will also be helpful for practical deployment at the entrance zone, since antenna and tag array can be easily deployed on the both sides of door.

## E. IMPACT OF ENVIRONMENT ASSOCIATED PARAMETERS

### 1) IMPACT OF SCENARIO

To check RFH's effectiveness under various scenarios, we further evaluate the estimation accuracy with different experimental scenarios as shown in Fig.12(a). We select three different scenarios in indoor environment, the left corner of hall, the right corner of hall and the center of a small water room. The size of hall is 6.0m  $\times$  14.2m and that of water room is only 3.3m  $\times$  3.4m. Fig.12(b) depicts the results of these three scenarios. As shown in the figure, the accuracy difference of RFH in left and right corner of hall is quite similar and subtle, the accuracy is larger than 90% in both scenarios with our EBOA optimization. However, the performance in the narrow water room is much lower. That is because of the rich multipath effect in a narrow environment, which suggests our RFH should be deployed in a open entrance zone to achieve much better performance.

### 2) IMPACT OF TAG TYPE

Finally, we evaluate the impact of tag type on the height estimation accuracy. We adopt three different types of tag in our

experiments, i.e., ImpinJ E41-C (type1), AZ-E53(type2) and H-47(type3). With all other parameters unchanged, Fig.12(c) plots the experimental results. According to the figure, the square ImpinJ H-47 tags achieves the best estimation accuracy larger than 98% among all the three types of tag. By contraries, the E41-C achieves the worst performance. The reason can be explained by coupling effect between tags in the array, whose spacing distance is 5cm only. The rectangle tags (E41-C and AZ-E53) usually have the line antennas in the tag, which causes serious coupling effect between adjacent tags when they are deployed close to each other. To overcome such impact of coupling effect, we'd better adopt the square shape tags in RFH.

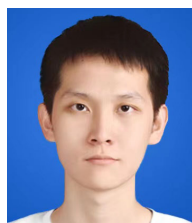
## VI. CONCLUSION

This work presents RFH, an low-cost RFID based height estimation solution, which is the first attempt to estimate entrant's height using passive and low cost RFID devices. Our key innovations lie in the RSSI changes caused by entrant's passing through can be a indicator of his/her height. With the identified influenced frames, we transform the signals into a strength image, so as to approximate entrant's height with foreground detection and centrum identification. Experimental results demonstrate that our RFH can achieve more than 80% accuracy in most cases. Although our solution still has great improvement space in terms of both accuracy and robustness, we believe our system will promote more possibilities of RFID-based sensing solution in practical deployments. In future work, we will combine the phase measurements of signals to model and analyze the entrant's height, which will possibly achieve a high accuracy.

## REFERENCES

- [1] J. Wang, D. Vasisht, and D. Katabi, "RF-IDraw: Virtual touch screen in the air using RF signals," in *Proc. ACM Conf. SIGCOMM*, Aug. 2014, pp. 235–246.
- [2] L. Yang, Y. Chen, X.-Y. Li, C. Xiao, M. Li, and Y. Liu, "Tagoram: Real-time tracking of mobile RFID tags to high precision using COTS devices," in *Proc. 20th Annu. Int. Conf. Mobile Comput. Netw.*, Sep. 2014, pp. 237–248.
- [3] L. Shangguan and K. Jamieson, "Leveraging electromagnetic polarization in a two-antenna whiteboard in the air," in *Proc. 12th Int. Conf. Emerg. Netw. EXperiments Technol.*, Dec. 2016, pp. 443–456.

- [4] G. Wang, C. Qian, L. Shanguan, H. Ding, J. Han, N. Yang, W. Xi, and J. Zhao, "HMRL: Relative localization of RFID tags with static devices," in *Proc. 14th Annu. IEEE Int. Conf. Sens., Commun., Netw. (SECON)*, Jun. 2017, pp. 1–9.
- [5] H. Ding, L. Shanguan, Z. Yang, J. Han, Z. Zhou, P. Yang, W. Xi, and J. Zhao, "FEMO: A platform for free-weight exercise monitoring with RFIDs," in *Proc. 13th ACM Conf. Embedded Netw. Sensor Syst.*, Nov. 2015, pp. 141–154.
- [6] J. Li, G. Feng, W. Wei, C. Luo, L. Cheng, H. Wang, H. Song, and Z. Ming, "PSOTrack: A RFID-based system for random moving objects tracking in unconstrained indoor environment," *IEEE Internet Things J.*, vol. 5, no. 6, pp. 4632–4641, Dec. 2018.
- [7] H. Ding, J. Han, A. X. Liu, J. Zhao, P. Yang, W. Xi, and Z. Jiang, "Human object estimation via backscattered radio frequency signal," in *Proc. IEEE Conf. Comput. Commun. (INFOCOM)*, Apr. 2015, pp. 1652–1660.
- [8] Z. Wang, N. Ye, R. Malekian, R. Wang, and P. Li, "TMicroscope: Behavior perception based on the slightest RFID tag motion," *Elektron. Elektrotech.*, vol. 22, no. 2, pp. 114–122, 2016.
- [9] X. Fan, W. Gong, and J. Liu, "i2tag: RFID mobility and activity identification through intelligent profiling," *ACM Trans. Intell. Syst. Technol.*, vol. 9, no. 1, pp. 1–21, Jan. 2018.
- [10] Y. Zheng, Y. He, M. Jin, X. Zheng, and Y. Liu, "RED: RFID-based eccentricity detection for high-speed rotating machinery," in *Proc. IEEE INFOCOM*, Apr. 2018, pp. 1565–1573.
- [11] Y. Bu, L. Xie, Y. Gong, C. Wang, L. Yang, J. Liu, and S. Lu, "RF-Dial: An RFID-based 2D human-computer interaction via tag array," in *Proc. IEEE INFOCOM*, Apr. 2018, pp. 837–845.
- [12] S. A. Vora, W. M. Mongan, E. K. Anday, K. R. Dandekar, G. Dion, A. K. Fontecchio, and T. P. Kurzweg, "On implementing an unconventional infant vital signs monitor with passive RFID tags," in *Proc. IEEE Int. Conf. RFID (RFID)*, May 2017, pp. 47–53.
- [13] U. Andriolo, D. Mendes, and R. Taborda, "Breaking wave height estimation from timex images: Two methods for coastal video monitoring systems," *Remote Sens.*, vol. 12, no. 2, p. 204, Jan. 2020.
- [14] W. Xinmei, X. Aijun, and Y. Tingting, "Passive measurement method of tree height and crown diameter using a smartphone," *IEEE Access*, vol. 8, pp. 11669–11678, 2020.
- [15] J. Wang, J. Xiong, X. Chen, H. Jiang, R. K. Balan, and D. Fang, "TagScan: Simultaneous target imaging and material identification with commodity RFID devices," in *Proc. 23rd Annu. Int. Conf. Mobile Comput. Netw.*, Oct. 2017, pp. 288–300.
- [16] A. Dhekne, M. Gowda, Y. Zhao, H. Hassanieh, and R. R. Choudhury, "LiquidID: A wireless liquid Identifier," in *Proc. 16th Annu. Int. Conf. Mobile Syst., Appl.*, Jun. 2018, pp. 442–454.
- [17] N. Sarafianos, B. Boteanu, B. Ionescu, and I. A. Kakadiaris, "3D human pose estimation: A review of the literature and analysis of covariates," *Comput. Vis. Image Understand.*, vol. 152, pp. 1–20, Nov. 2016.
- [18] M. Asadi-Aghbolaghi, A. Clapes, M. Bellantonio, H. J. Escalante, V. Ponce-Lopez, X. Baro, I. Guyon, S. Kasaei, and S. Escalera, "A survey on deep learning based approaches for action and gesture recognition in image sequences," in *Proc. 12th IEEE Int. Conf. Autom. Face Gesture Recognit. (FG)*, May 2017, pp. 476–483.
- [19] G. Pons-Moll and B. Rosenhahn, "Model-based pose estimation," in *Visual Analysis of Humans*. London, U.K.: Springer, 2011, pp. 139–170.
- [20] G. Pavlakos, X. Zhou, and K. Daniilidis, "Ordinal depth supervision for 3D human pose estimation," in *Proc. IEEE/CVF Conf. Comput. Vis. Pattern Recognit.*, Jun. 2018, pp. 7307–7316.
- [21] G. Pons-Moll, J. Taylor, J. Shotton, A. Hertzmann, and A. Fitzgibbon, "Metric regression forests for correspondence estimation," *Int. J. Comput. Vis.*, vol. 113, no. 3, pp. 163–175, 2015.
- [22] S. Chu and J. Tanaka, "Hand gesture for taking self portrait," in *Proc. ICHI*, 2011, pp. 238–247.
- [23] Y. Madhuri, G. Anitha, and M. Anburajan, "Vision-based sign language translation device," in *Proc. Int. Conf. Inf. Commun. Embedded Syst. (ICICES)*, Feb. 2013, pp. 565–568.
- [24] J. L. Raheja, A. Chaudhary, and K. Singal, "Tracking of fingertips and centers of palm using KINECT," in *Proc. 3rd Int. Conf. Comput. Intell., Modeling Simulation*, Sep. 2011, pp. 248–252.
- [25] Y. Ma, G. Zhou, and S. Wang, "WiFi sensing with channel state information: A survey," *ACM Comput. Surv.*, vol. 52, no. 3, pp. 1–36, Jul. 2019.
- [26] F. Adib and D. Katabi, "See through walls with WiFi!" in *Proc. ACM SIGCOMM*, Aug. 2013, pp. 75–86.
- [27] C. Han, K. Wu, Y. Wang, and L. M. Ni, "WiFall: Device-free fall detection by wireless networks," in *Proc. IEEE INFOCOM*, Apr. 2014, pp. 581–594.
- [28] L. Gong, W. Yang, D. Man, G. Dong, M. Yu, and J. Lv, "WiFi-based real-time calibration-free passive human motion detection," *Sensors*, vol. 15, no. 12, pp. 32213–32229, 2015.
- [29] S. Arshad, C. Feng, Y. Liu, Y. Hu, R. Yu, S. Zhou, and H. Li, "Wi-chase: A WiFi based human activity recognition system for sensorless environments," in *Proc. IEEE 18th Int. Symp. World Wireless, Mobile Multimedia Netw. (WoWMoM)*, Jun. 2017, pp. 1–6.
- [30] W. Wang, A. X. Liu, M. Shahzad, K. Ling, and S. Lu, "Device-free human activity recognition using commercial WiFi devices," *IEEE J. Sel. Area Commun.*, vol. 35, no. 5, pp. 1118–1131, Mar. 2017.
- [31] K. Qian, C. Wu, Y. Zhang, G. Zhang, Z. Yang, and Y. Liu, "Widar2.0: Passive human tracking with a single Wi-Fi link," in *Proc. ACM Mobisys*, 2018, pp. 350–361.
- [32] X. Liu, J. Cao, S. Tang, J. Wen, and P. Guo, "Contactless respiration monitoring via off-the-shelf WiFi devices," *IEEE Trans. Mobile Comput.*, vol. 15, no. 10, pp. 2466–2479, Oct. 2016.
- [33] A. Kalyanaraman, D. Hong, E. Soltanaghaei, and K. Whitehouse, "Forma track: Tracking people based on body shape," in *Proc. ACM Ubicomp*, 2017, vol. 1, no. 3, p. 61.
- [34] L. Yang, Q. Lin, X. Li, T. Liu, and Y. Liu, "See through walls with COTS RFID system!" in *Proc. 21st Annu. Int. Conf. Mobile Comput. Netw.*, Sep. 2015, pp. 487–499.
- [35] Y. Hou, Y. Wang, and Y. Zheng, "TagBreathe: Monitor breathing with commodity RFID systems," in *Proc. IEEE 37th Int. Conf. Distrib. Comput. Syst. (ICDCS)*, Jun. 2017, pp. 404–413.
- [36] A. Rashee, E. Iranmanes, W. Li, X. Fen, A. S. Andrenk, and K. Wan, "Experimental study of human body effect on temperature sensor integrated RFID tag," in *Proc. IEEE Int. Conf. RFID Technol. Appl. (RFID-TA)*, Sep. 2017, pp. 243–247.
- [37] J. Liu, X. Chen, S. Chen, X. Liu, Y. Wang, and L. Chen, "TagSheet: Sleeping posture recognition with an unobtrusive passive tag matrix," in *Proc. IEEE INFOCOM*, Apr. 2019, pp. 874–882.
- [38] (2018). *Impinj*. [Online]. Available: <http://www.impinj.com>
- [39] K. U. Shajeeh, S. Sachin Kumar, D. Pravena, and K. P. Soman, "Speech enhancement based on Savitzky-Golay smoothing filter," *Int. J. Comput. Appl.*, vol. 57, no. 21, pp. 39–44, 2012.



**YUQIU ZHAO** is currently pursuing the B.S. degree with the College of Computer and Information Engineering, Central South University of Forestry and Technology. He was a Visiting Student at Yanshan University, in Summer 2021. His research interest includes the Internet of Things (IoT).



**JIANCHAO LI** received the B.S. degree in software engineering from the Industrial and Commercial College, Hebei University, in 2017, and the M.E. degree in software engineering from Yanshan University, in 2021. His research interest includes RFID.



**WENYUAN LIU** received the B.S. and M.E. degrees in computer science from the Northeast Heavy Machinery Institute, China, and the Ph.D. degree in computer science from the Harbin Institute of Technology, in 2000. Since 1996, he has been with the School of Information Science and Engineering, Yanshan University, Qinhuangdao, China, where he is currently a Professor. His research interests include wireless sensor networks and mobile networks.